Theory of attosecond time delay in double photoionization of noble gas atoms

J. M. Dahlström* and E. Lindroth
Department of Physics, Stockholm University, AlbaNova University Center, SE-106 91 Stockholm, Sweden

M. Gisselbrecht and A. L'Huillier
Department of Physics, Lund University, P.O. Box 118, 22100 Lund, Sweden

A. S. Kheifets†
Research School of Physical Sciences, The Australian National University, Canberra ACT 0200, Australia

(Dated: June 4, 2013)

We present a theoretical interpretation of attosecond time-delays in double photoionization (DPI) measured in XUV-pump and IR-probe experiments using coincidence detection. The so-called Wigner time delay is extended to DPI and serves as a guide to better understand the observable time-delay in the two-color case. By employing diagrammatic perturbation theory, we derive explicit corrections to the time delays in DPI due to many-electron correlations and due to the effect of the probing IR field. The present theory can be applied to closed-shell atomic targets like noble gas atoms. We give specific numerical estimates for the time delay in DPI of the outer np^6 shell of Xe and make a comparison with a recent experimental data [Månsson *et al.*, Nature, submitted (2013)]

I. INTRODUCTION

Single-photon two-electron ionization of an atom, referred to as atomic double photoionization (DPI), represents the most fundamental atomic collision process driven entirely by electron correlation. Since one photon can only couple to one electron, the secondary electron must be removed by various correlation mechanisms. Because of this clear manifestation of many-electron correlation, atomic DPI has long and extensively been studied, both theoretically and experimentally [1, 2]. The two specific correlation mechanisms, the shake-off (SO) and knock-out (KO) (also called "two-step-one") processes have been identified [3] and their relative contribution was separated in helium [4]. These studies, however, have been confined to the static regime in which the timing information about the DPI process was not accessible. Implicitly, it is presumed that the SO process, in which the secondary photoelectron is shaken off after a sudden rearrangement of the ionic core, is fast. On the contrary, the KO process, in which the secondary photoelectron is knocked off by the primary photoelectron in an ionizing collision, is relatively slow. Hence, the SO process eventually takes over with the increase of the photon energy and emission of the increasingly fast primary photoelectron [5].

Recently, with the advent of attosecond science, experimental schemes have been designed for time-resolved studies of single electron emission from an atom - the process that we refer to as single photoionization (SPI) [6–8]. In these schemes, the photoelectron is ejected from an atom by a single attosecond pulse of extreme ultraviolet (XUV) radiation, whereas the timing information is obtained by superimposing a phase-locked infrared (IR) probe pulse. In attosecond streaking experiments [6], the time delay between the XUV pulse and a short IR pulse of a few oscillations is mapped onto the momentum of the photoelectron in the form of a *spectrogram.* The time delay is then extracted by using the strong field approximation (SFA) which relates the unperturbed asymptotic momentum of the photoelectron $\boldsymbol{p}_0$ and the final momentum $\boldsymbol{p}_f(t)$ for emission at time t in the presence of an IR field $\boldsymbol{A}^{\rm IR}$:

$$\boldsymbol{p}_f(t) \approx \boldsymbol{p}_0 - \boldsymbol{A}^{\rm IR}(t) \ . \tag{1}$$

An alternative set of attosecond time delay measurements [7, 8] employs attosecond pulse trains and a monochromatic IR probe. These experiments utilized the so-called RABITT (Reconstruction of Attosecond Bursts by Ionization of Two-photon Transitions) technique. This technique consists in recording a spectrogram as a function of the photoelectron energy and the relative delay between the train of attosecond pulses and the weak IR probe [9]. The pump-probe delay is mapped onto the phase of the sideband oscillations caused by interference of alternative two-photon ionization processes.

A more elaborate theoretical interpretation of the attosecond time delay measurements in SPI takes into account the interplay of an IR field with the long-range Coulomb potential of the ionic core, the so-called Coulomb-laser coupling (CLC) [10, 11]. This effect leads to modification of Eq. (1) to the following form

$$\boldsymbol{p}_f(t) \approx \boldsymbol{p}_0 - \alpha \boldsymbol{A}^{\rm IR}(t+t_{\rm S}) \ . \tag{2}$$

Here α is a correction factor for the amplitude of the momentum shift induced by the streaking field, and the time delay measured in attosecond streaking experiments is split into two contributions:

$$\tau_{\rm S} = \tau_{\rm W} + \tau_{\rm CLC} \ . \tag{3}$$

Here $\tau_{\rm W}$ is the photoelectron group delay, also known as the Wigner time delay, which is defined as the energy derivative of the complex phase of the quantum amplitude of XUV absorption [6, 12]. An additional term $\tau_{\rm CLC}$ arises due to the Coulomb-laser coupling. Similar to Eq. (3), the atomic time delay measured in RABITT experiments can be presented as

$$\tau_{\rm A} = \tau_{\rm W} + \tau_{\rm cc} \ . \tag{4}$$

---

*Electronic address: `Marcus.Dahlstrom@fysik.su.se`
†Electronic address: `A.Kheifets@anu.edu.au`

Here $\tau_{\rm cc}$ is the time delay due to the complex phase of the matrix element of the IR photon absorption (the continuum–continuum or "cc" transition). For a weak IR probe, this term can be modeled using lowest-order perturbation theory [13, 14]. It has been demonstrated analytically that the IR-induced delays are equal, $\tau_{\rm CLC} = \tau_{\rm cc}$, provided that the IR intensity is weak. In this sense, the delay in streaking experiments also originates from the same phase-shift of the two-photon (XUV+IR) matrix element, c.f. Ref. [13].

Further, it has been shown that correlated two-electron atomic transitions, such as single photoionization with excitation (shake-up), lead to modifications of the streaking time delay, Eq. (3), by electron-electron polarization effects [16]:

$$\tau_{\rm S} = \tau_{\rm W} + \tau_{\rm CLC} + \tau_{\rm CLC}^{ee} \ . \tag{5}$$

In contrast to the numerous and detailed time-resolved studies of SPI, the timing analysis of DPI has been limited so far. The only published theoretical work [15] analyzed DPI of He in the attosecond streaking configuration without an explicit account for the probing IR field. A recently completed experimental work [17] probed the DPI of the $5p^6$ shell of xenon on the attosecond time scale using the RABITT technique. As a reference clock in this experiment, the SPI of the same shell was used. The latter was modeled theoretically using Eq. (4) in which the Wigner time delay was extracted from the calculation [18] that accounted for inter-shell correlation. The result was, quite counter-intuitively, that the DPI and SPI processes from the outer shell of Xe showed no significant relative delay within the experimental uncertainty. This finding was interpreted in Ref. [17] in terms of the leading DPI mechanisms using diagrammatic perturbation theory.

The purpose of the present work is two-fold. First, we want to extend the definition of the Wigner time delay in XUV driven photoionization to the DPI process and to evaluate its specific components due to individual photoelectrons group delay and their mutual correlation. Second, we want to describe the effect of the probing IR field on these individual and correlated components of the time delay. We employ the lowest order perturbation theory valid for closed shell atomic targets like noble gas atoms. We give specific numerical estimates for the time delay in DPI of the outer np^6 shell of Xe and make a comparison with a recent experiment [17]. A brief account of our theory was published alongside the experimental data. Here, we present our results in considerably more detail.

The present paper is organized as follows. In Sec. II, we outline the key ingredients of the experimental technique. In Sec. II A we recall the theoretical interpretation of the time delay measurement in SPI. In Sec. II B we extend this interpretation to DPI based on general properties of the ionization amplitude. In Sec. III we consider specific mechanisms of DPI. In Sec. III A we perform a diagrammatic analysis of the laser-assisted shake-off and knock-out mechanisms in DPI. In both cases, we show explicitly that the experimental observable is the sum of the time delay in DPI, as derived empirically in Sec. II B, but it also includes a correction due to the IR probing process. In Sections III B 1 and **??** we give correlation corrections to the time delay which are specific to the shake-off and knock-out mechanisms, respectively. In Section III B 2 we give numerical estimates for the interaction strength with the probe field. In Sec. IV we make a comparison with the available experimental data for Xe reported in [17]. Finally, in Sec. V we conclude by outlining possible extensions of the present work and the future directions of time delay studies of multiple atomic ionization. The atomic units are used throughout the paper.

II. RABITT TECHNIQUE

A. RABITT measurement of single ionization

A detailed introduction to the RABITT method for time delay studies in SPI is found in Refs. [13, 23]. The probability modulation of a sideband $2q$ in a RABITT spectrogram is given by

$$S_{2q}(\tau) \propto \cos(2\omega\tau - \Delta\phi_{2q} + \Delta\theta_{2q}) \ .$$

Here ω is the IR photon frequency, τ is the time delay between the the XUV and IR fields, $\Delta\phi_{2q}$ denotes the phase difference between the two harmonics with order $2q+1$ and $2q-1$, while $\Delta\theta_{2q}$ is the phase difference between the two quantum paths leading to the final energy. The photoelectron may either absorb a photon from the harmonic order $2q-1$ plus a probe photon or it may absorb a photon from the harmonic $2q+1$ and emit a probe photon. We may relate the harmonic phase difference to an approximate group delay of the attosecond pulses $\tau_{\rm GD} \approx \Delta\phi_{2q}/2\omega$ relative to the zero-time for the ionization process. Similarly, we may define the atomic delay $\tau_{\rm A} = \Delta\theta_{2q}/2\omega$, which describes an additional delay inherent to the two-photon ionization process. As mentioned above, in connection with Eq. (4), the latter includes a Wigner-like delay,

$$\tau_{\rm W} \equiv \frac{d\varphi}{d\Omega} \approx \frac{\varphi(\epsilon+\omega) - \varphi(\epsilon-\omega)}{2\omega} \ , \tag{6}$$

corresponding to an XUV frequency between the odd harmonics, $\Omega \approx 2q\omega$. In Eq. (6), a finite difference approximation is made to the energy derivative of the complex phase $\phi = \arg M_{\rm SPI}(\boldsymbol{p})$ of the angle-resolved matrix element of SPI leaving the photoelectron in the momentum state $\boldsymbol{p}$, with energy $\epsilon = p^2/2$. In the single active electron approximation, this phase can be related to the elastic scattering phase η_λ of the photoelectron on the residual ion in the dominant angular channel λ (see Eq. (15) in Sec. III A). A more general expression includes an addition term due to the inter-shell correlation (c.f. Eq. (20) of Guénot et al. [8])

$$\tau_{\rm W} \equiv \frac{d\phi}{d\epsilon} = \frac{d\eta_\lambda}{d\epsilon} + \frac{d\delta_\lambda}{d\epsilon}. \tag{7}$$

B. Wigner-like delay in DPI

In this subsection we define the Wigner delay component, $\tau_{\rm W}$, in the DPI process. Similar to Eq. (7), it is equivalent to the XUV photon energy derivative of the phase of the amplitude of the DPI process

$$\tau_{\rm W}^{\rm (DPI)} = \frac{\partial}{\partial\Omega} \arg M_{\rm DPI}(\boldsymbol{p},\boldsymbol{q}) \ , \tag{8}$$

leading to the two photoelectrons $\boldsymbol{p}$ and $\boldsymbol{q}$. The excess energy above the double ionization threshold, $E = \Omega - I_{\rm DI}$, and the energy difference, ΔE, are related to the energy of the individual electrons, (ϵ_p, ϵ_q), as

$$\begin{pmatrix} E \\ \Delta E \end{pmatrix} = \begin{pmatrix} 1 & 1 \\ 1 & -1 \end{pmatrix} \begin{pmatrix} \epsilon_p \\ \epsilon_q \end{pmatrix} . \qquad (9)$$

We make a linear transformation of Eq. (9) to the individual electron energies and find that a change of the total energy (here, given by the XUV photon) is

$$\frac{\partial}{\partial \Omega} = \frac{\partial}{\partial E} = \frac{1}{2}\frac{\partial}{\partial \epsilon_p} + \frac{1}{2}\frac{\partial}{\partial \epsilon_q} \ , \qquad (10)$$

while the energy difference is unchanged. If we are able to isolate the dominant channels in the angular momentum expansion of both photoelectrons, then we can write the phase of the DPI amplitude as

$$\arg M_{\rm DPI} = \eta_{\lambda_p}(\epsilon_p) + \eta_{\lambda_q}(\epsilon_q) + \delta^{\rm (ee)}_{\lambda_p,\lambda_q}(\epsilon_p, \epsilon_q) \ , \qquad (11)$$

where the first two terms in the right-hand side are the elastic scattering phases of the two photoelectrons (as in SPI) and the third term is due to their correlation. The DPI version of Eq. (7) can thus be written as

$$\tau_{\rm W}^{\rm (DPI)} = \frac{1}{2}\left[\frac{\partial \eta_{\lambda_p}}{\partial \epsilon_p} + \frac{\partial \eta_{\lambda_q}}{\partial \epsilon_q} + \frac{\partial \delta^{\rm (ee)}_{\lambda_p,\lambda_q}}{\partial \epsilon_p} + \frac{\partial \delta^{\rm (ee)}_{\lambda_p,\lambda_q}}{\partial \epsilon_q} \right] , \qquad (12)$$

which we may interpret as the average Wigner-like delay of the two electrons plus correction terms due to their correlation.

III. DPI MECHANISMS

A. Diagram analysis

In Fig. 1 (a)–(h) we present the time-ordered Feynman-Goldstone diagrams for double ionization by absorption of one or two photons. These processes result in a primary photoelectron, p, and a secondary electron, q, both with positive energy, ϵ_p, $\epsilon_q > 0$. Consequently, the atom is left with two remaining holes, a and b, with ϵ_a, $\epsilon_b < 0$. The lowest-order perturbation diagrams for the SO and KO processes following absorption of one XUV photon are shown in Fig. 1 (a) and (e), respectively, where energy conservation is enforced on the outgoing particles,

$$E = \epsilon_p + \epsilon_q = \epsilon_a + \epsilon_b + \Omega. \qquad (13)$$

The corresponding laser-assisted processes, LASO and LAKO, where an additional IR photon is exchanged by one of the photoelectrons, are shown in Fig. 1 (b)–(d) and (e)–(h), respectively. In these two-photon processes energy conservation must be enforced,

$$E = \epsilon_p + \epsilon_q = \epsilon_a + \epsilon_b + \Omega \pm \omega, \qquad (14)$$

for either absorption $(+\omega)$ or emission $(-\omega)$ of an IR photon. We will limit our analysis to the dominant processes that are initiated by absorption of one XUV photon and then probed by one IR photon, i.e. we neglect all interactions of the IR field with the initial state and with the holes. However, there are still three distinct mechanisms for how the IR photon can interact with the excited system. The IR photon may interact with the primary photoelectron *before* double ionization has occurred, Fig. 1 (b) and (f), or it may interact with the either of the electrons *after* double ionization has occurred, Fig. 1 (c)–(d) and (g)–(h). In this way, the SPI process is imprinted on the DPI process in a nontrivial way by the interaction with the IR probe field.

The states in Fig. 1 are written with short-hand notation for a spherical basis, e.g. $|p\rangle \equiv |k_p, L_p, M_p\rangle$, where the quantum number p stands for the complete set of orbital quantum numbers (explicit account for the spin is not given here since all interaction are spin-independent). We use the following phase-convention for the continuous energy states

$$\psi_p(\boldsymbol{r}) \equiv \langle \boldsymbol{r}|p\rangle \equiv \exp(-i\eta_p)\frac{u_{k_p,L_p}(r)}{r} Y_{L_p,M_p}(\boldsymbol{r}/r) \ , \qquad (15)$$

which ensures that the outgoing part of the real radial states, $u_p(r) \equiv u_{k_p,L_p}(r)$, form an uniform phase front with the Coulombic logarithmic diverging phase, $k_p r + Z\ln(2k_p r)/k$, where Z is the effective charge of the ion after ionization. The asymptotic phase-shift of the energy state with angular momentum L_p,

$$\eta_p \ \equiv \ -\tfrac{\pi}{2}L_p \ + \ \sigma(L_p, k_p) \ + \ \delta(L_p, k_p) \ , \qquad (16)$$

includes the centrifugal phase, the hydrogenic phase and the phase-shift due to an ionic potential (static plus exchange), respectively.

In this work we will consider angle-integrated energy states, Eq. (15), that were the observables in the recent experiment on laser-assisted double photoionization by attosecond pulses [17]. For simplicity we will also assume that one final angular momentum pair to dominant.

1. Shake-off mechanism (SO)

The equation for the SO diagram in Fig. 1 (a) is

$$M_{\rm SO}^{(a,b;p,q)}(\epsilon_p, \epsilon_q) = -\sum_c \frac{\langle p|d_\Omega|c\rangle\langle cq|r_{12}^{-1}|ab\rangle}{(\epsilon_c + \Omega - \epsilon_p)}, \qquad (17)$$

where the primary electron, p with energy ϵ_p, is ejected from any occupied atomic state, c, by absorption of one XUV photon, Ω. Then the corresponding hole, c, by way of the Coulomb interaction, undergoes an Auger decay into two holes, (a, b), and a secondary electron, q with energy ϵ_q, is "shaken off". We mention that the divergence that occurs in Eq. (17) for $\epsilon_p = \epsilon_c + \Omega$ is artificial and reduced to a finite peak when higher-order corrections are included, c.f. Ref. [24].

	$5p^{-1}$	$2 \times 5p^{-1}$	$5p^{-2}$	$5s^{-1}$	$4d^{-1}$
$\epsilon_{\rm exp}$ (eV)	-12.1	-24.2	-33.1	-23.3	-67.5

TABLE I: Experimental energies of holes in xenon [25].

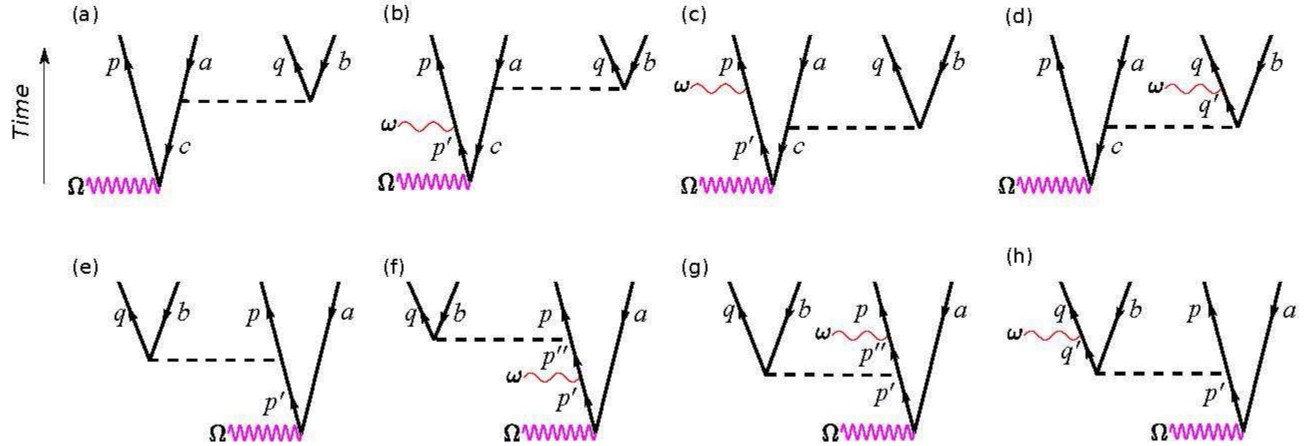

FIG. 1: Lowest-order perturbation diagrams for the shake-off (SO) process (a); laser-assisted shake-off (LASO) processes (b)–(d); the knock-out (KO) process (e); and laser-assisted knock-out (LAKO) processes (f)–(h). The holes (a, b, c) are represented by down arrows (↓), while the primary (p) and secondary (q) electrons are drawn with up arrows (↑). The XUV photon and the IR photon are fast and slow wiggles, respectively, while the Coulomb interaction is a dashed line. Summation over all primed electron states and the core (c) is implied.

Here, we will consider the case of a virtual Auger decay, $\epsilon_q \approx \epsilon_a + \epsilon_b - \epsilon_c < 0$, which is typical of outer atomic shells. As an example, we review the Xe atom where the final holes a and b are located in the outer-most sub-shell $5p$, see Table. I. The binding of the two interacting holes is even greater than the sum of their individual energies. This ensures that the secondary electron can not easily escape (autoionize), instead, it is the "shake-up" that is the domiant (on shell) process. However, there is a small probability for the the emission of a secondary electron by the SO process due to energy sharing in the double ionization process, Eq. (14). According to Table. I, the secondary electron must "borrow" at least 9.8 eV in order to escape via $c = 5s^{-1}$ leaving the $5p^{-2}$ state behind. We will not consider autoionization, e.g. via $c = 4d^{-1}$, where the binding of the hole is sufficient to create two holes in the outer valence in an on shell-process, $\epsilon_{5p}+\epsilon_{5p}-\epsilon_{4d} > 0$.

2. *Laser-assisted shake-off mechanism (LASO)*

We proceed by considering the various diagrams of the LASO process, Fig. 1 (b)–(d). First, we note that the two time-orders for the IR interaction with the primary electron, Fig. 1 (b) and (c), have identical structure and, therefore, only differ in their energy denominators. Making use of energy conservation for the final state, Eq. (14), these two diagrams can be joined into one effective matrix element,

$$M^{(p)}_{\mathrm{LASO}}(\epsilon_p, \epsilon_q) = - \sum_{c,p'} \frac{\langle p|d_\omega|p'\rangle\langle p'|d_\Omega|c\rangle\langle cq|r_{12}^{-1}|ab\rangle}{(\epsilon_c - \epsilon_a - \epsilon_b + \epsilon_q)(\epsilon_p \mp \omega - \epsilon'_p)}. \tag{18}$$

The first factor in the denominator of Eq. (18) is of "Auger type" and it similarly describes the (virtual) decay of a hole, c, into two holes, (a, b), and one electron, q. This denominator is identical to the SO process, if we substitute Ω in Eq. (17) using Eq. (13).

The second factor in Eq. (18) is related to the intermediate state of the primary electron, as it interacts with the IR field. Similar to the laser-assisted one-electron ionization process, this transition occurs from an outgoing Coulombic wave of the energy shifted by one IR photon relative to the final state energy, $\epsilon_{p'} = \epsilon_p \mp \omega$, for IR absorption and emission, respectively. The details of this above-threshold transition is identical to that of the "cc" transition in SPI and, therefore, leads to a cc phase-shift, c.f. Ref. [13]. The phase of LASO for the primary electron (p) contains

$$\arg M^{(p)}_{\mathrm{LASO}} \sim \varphi_p(\epsilon_p \mp \omega) + \phi_{\mathrm{cc}}(\epsilon_p; \pm\omega) + \varphi_q(\epsilon_q), \tag{19}$$

where the scattering phase of the primary photoelectron is evaluated at one IR photon away from the final energy, while the scattering phase of the secondary electron is that of the final energy [quantum numbers correspond to Fig. 1 (a)].

In Fig. 1 (d) the secondary electron, q, is probed by LASO. Using energy conservation, Eq. (14), the corresponding denominator,

$$M^{(q)}_{\mathrm{LASO}}(\epsilon_p, \epsilon_q) = \sum_{c,q'} \frac{\langle q|d_\omega|q'\rangle\langle cq'|r_{12}^{-1}|ab\rangle\langle p|d_\Omega|c\rangle}{(\epsilon_c - \epsilon_a - \epsilon_b + \epsilon_q \mp \omega)(\epsilon_q \mp \omega - \epsilon'_q)}, \tag{20}$$

reveals that the secondary electron is shaken off with an intermediate energy, $\epsilon_{q'} = \epsilon_q \mp \omega$, and then transitions to the final state, q, by interaction with the IR field. The phase of the LASO for the secondary electron (q) contains

$$\arg M^{(q)}_{\mathrm{LASO}} \sim \varphi_p(\epsilon_p) + \varphi_q(\epsilon_q \mp \omega) + \phi_{\mathrm{cc}}(\epsilon_q; \pm\omega), \tag{21}$$

where the phase of the primary electron is that of the final energy, while the phase of the secondary electron is evaluated at one IR photon energy away from the final state [quantum numbers correspond to Fig. 1 (a)].

The total LASO process, $M_{\mathrm{LASO}}(a, b; p, q; \Omega, \omega)$, is a superposition of both processes,

$$|M_{\mathrm{LASO}}| \exp(i\Phi_{\mathrm{LASO}}) = M^{(p)}_{\mathrm{LASO}} + M^{(q)}_{\mathrm{LASO}}, \tag{22}$$

where the IR field interacts with the primary or secondary electron. For simplicity, we consider only the dominant process, where the primary electron is faster than the secondary electron, $\epsilon_p > \epsilon_q$. The total LASO matrix element can be rewritten as

$$M = \exp(i\bar{\Phi}) \times 2\big(\bar{M}\cos\Delta\Phi + i\Delta M \sin\Delta\Phi\big), \tag{23}$$

where we temporarily suppressed the subscript LASO for brevity and the average and difference phases are defined as

$$\begin{aligned}\bar{\Phi} &= \tfrac{1}{2}(\arg M^{(p)} + \arg M^{(q)}) \\ \Delta\Phi &= \tfrac{1}{2}(\arg M^{(p)} - \arg M^{(q)}).\end{aligned} \tag{24}$$

The corresponding magnitudes for average, $\bar{M}$, and difference, ΔM, in Eq. (23) are defined in an analogous way. According to Eq. (23), the total phase of the LASO matrix element depends on the relative strength of the two processes in much the same way as the interference of two laser beam depends on their respective strength.

In order to estimate the relative strength of the two contributions, $|M^{(p)}_{\mathrm{LASO}}|$ and $|M^{(q)}_{\mathrm{LASO}}|$, we turn to the strong field approximation (SFA). The IR field can "streak" the photoelectron in energy by

$$\Delta\epsilon \approx -p_0 A^{\mathrm{IR}}(t)\ , \tag{25}$$

where p_0 is the magnitude of the final momentum (without IR) along the polarization axis of the vector potential. This expression is obtained by squaring Eq. (1) and keeping the term linear in $A^{\mathrm{IR}}(t)$. In this sense, the interaction with the IR field gives the electron a boost in energy that is linear with its own momentum. Quantum mechanically, the *on-set* of streaking can be performed using the photon picture [13]. By combining these two view points, we derive that the quantum mechanical amplitude of the IR induced transition is

$$|a_{\mathrm{cc}}| \approx \frac{p_0}{2\omega^2}, \tag{26}$$

where the IR absorption strength is indeed linear with the momentum of the ejected electron, but the interaction strength also increases strongly as the frequency of IR field is reduced. A more detailed numerical estimate will be given in Sec. III B 2, where we show that this linear behavior is a good approximation for high momentum of the photoelectron.

Using Eq. (26), the magnitudes of the LASO process can be approximated as

$$\begin{aligned}\bar{M}_{\mathrm{LASO}} &\approx \tfrac{1}{2}\,|M_{\mathrm{SO}}| \times \frac{p_0(\epsilon_p)+p_0(\epsilon_q)}{2\omega^2} \\ \Delta M_{\mathrm{LASO}} &\approx \tfrac{1}{2}\,|M_{\mathrm{SO}}| \times \frac{p_0(\epsilon_p)-p_0(\epsilon_q)}{2\omega^2},\end{aligned} \tag{27}$$

where $|M_{\mathrm{SO}}|$ is the magnitude of the SO process (without IR field present), which will be discussed further in Sec. III B 1.

By inserting Eq. (27) into Eq. (23), we identify that the phase of the total LASO process,

$$\Phi = \bar{\Phi} + \underbrace{\operatorname{atan}\left[\frac{p_0(\epsilon_p)-p_0(\epsilon_q)}{p_0(\epsilon_p)+p_0(\epsilon_q)}\tan\Delta\Phi\right]}_{\delta\Phi_{\mathrm{weight}}}, \tag{28}$$

is the sum of the average LASO phase and a phase weight correction, $\delta\Phi_{\mathrm{weight}}$, that accounts for the different IR interaction strengths of the two electrons. At equal energy sharing, we have $p_0(\epsilon_p) = p_0(\epsilon_q) \rightarrow \delta\Phi_{\mathrm{weight}} = 0$, and the LASO phase will reduce to the average phase of the two individual processes, $\bar{\Phi}$. In the other limit, when $p_0(\epsilon_p) \gg p_0(\epsilon_q)$, the correction phase turns the total phase into that of the primary electron, Eq. (19), and the LASO process becomes insensitive to the phase of the slower electron.

In order to determine the experimental observable of an angle-integrated experiment, we must add all complex amplitudes leading to the same final states, $(a,b;p,q)$, including both absorption, $M^{(\mathrm{abs})}_{\mathrm{LASO}} = M_{\mathrm{LASO}}(\Omega_{2q-1},\omega)$, and emission, $M^{(\mathrm{emi})}_{\mathrm{LASO}} = M_{\mathrm{LASO}}(\Omega_{2q+1},-\omega)$, of a probe photon. These amplitudes are squared together and the observable delay is identified from the crossterm (analogous to the SPI RABITT method)

$$\begin{aligned}\tau_{\mathrm{LASO}} =& \frac{\mathit{\Phi}^{(\mathrm{emi})}_{\mathrm{LASO}} - \mathit{\Phi}^{(\mathrm{abs})}_{\mathrm{LASO}}}{2\omega} \\ =& \tfrac{1}{2\omega}\big\{\big[\varphi_p(\epsilon_p+\omega) - \varphi_p(\epsilon_p-\omega) \\ &+\varphi_q(\epsilon_q+\omega) - \varphi_q(\epsilon_q-\omega) \\ &+\phi_{\mathrm{cc}}(\epsilon_p;-\omega) - \phi_{\mathrm{cc}}(\epsilon_p;\omega) \\ &+\phi_{\mathrm{cc}}(\epsilon_q;-\omega) - \phi_{\mathrm{cc}}(\epsilon_q;\omega)\big] \times \tfrac{1}{2} \\ &+\delta\Phi^{\mathrm{LASO}}_{\mathrm{weight}}(-\omega) - \delta\Phi^{\mathrm{LASO}}_{\mathrm{weight}}(\omega)\big\},\end{aligned} \tag{29}$$

relative to the group delay of the attosecond pulse centered of XUV frequency $\Omega_{2q} = \epsilon_p + \epsilon_q - \epsilon_a - \epsilon_b$ [quantum numbers correspond to Fig. 1 (a)]. By applying the finite-difference derivatives for the phase variations and the definition of the cc-delay [13], we obtain the two-electron average of the Wigner delay and cc-delay, plus an IR-weighting term,

$$\tau_{\mathrm{LASO}} \approx \tfrac{1}{2}[\tau^{(p)}_{\mathrm{W}} + \tau^{(q)}_{\mathrm{W}} + \tau^{(p)}_{\mathrm{cc}} + \tau^{(q)}_{\mathrm{cc}}] + \delta\tau^{\mathrm{LASO}}_{\mathrm{weight}}. \tag{30}$$

The probing process by the IR field does give access to the average Wigner delay of the two electrons as expected from Eq. (12), but it also introduces an average cc-delay that is quite similar to the SPI case. Unlike SPI, however, an effect rises in DPI due to respective interaction strengths with the IR field of two electrons. Our derivation shows that this effect is zero at equal energy sharing, where both electrons interact equally with the IR field. However, as one electron becomes faster, the total LASO delay will only give information about that particular electron.

These lowest-order results can only be regarded as the starting point for the analysis of RABITT type measurements in DPI. In order to include more correlation we may incorporate RPAE-type corrections, as was shown in Eq. (7) for SPI. For the primary electron such a procedure is adequate, but for the secondary electron, the effective charge of the nucleus will be greater ($Z_{\mathrm{eff}} \approx 2$), so that further correlation must be considered. These effects are consistent with our heuristic analysis, where we introduced the additional $\delta^{(\mathrm{ee})}_{\lambda_p,\lambda_q}(\epsilon_p,\epsilon_q)$. Similarly, the cc-delays will be affected by the effective charge of the ion, where the secondary electron will absorb the IR photon in an ionic potential of $Z_{\mathrm{eff}} \approx 2$, rather than $Z_{\mathrm{eff}} \approx 1$. Electron–electron interaction may further influence this screening, provided that their kinetic energies are not too different. Finally, a substantial SO process may involve additional virtual Coulomb interactions which will be discussed further in Sec. III B 1.

In angle-integrated experimental measurements, not all degrees of freedom are observed and it is necessary to sum incoherently all individual probabilities for each angular paths. In addition, the cases where the secondary electron is faster than the primary, i.e. when $\epsilon_q = \epsilon_p > \epsilon_p = \epsilon_q$. This individual contribution is easily achieved by interchanging ϵ_p and ϵ_q in Eq. (38).

3. Knock-out mechanism (KO)

The equation for the KO process in Fig. 1 (e) is

$$M_{\mathrm{KO}}^{(a,b;p,q)}(\epsilon_p, \epsilon_q) = \lim_{\varepsilon\to 0^+} \sum\!\!\!\!\!\!\!\int_{p'} \frac{\langle qp|r_{12}^{-1}|bp'\rangle\langle p'|d_\Omega|a\rangle}{\epsilon_a + \Omega - \epsilon'_p + i\varepsilon}, \quad (31)$$

where the primary electron, p', is ejected from the occupied atomic state, a, by absorption of one XUV photon, Ω. Then the primary electron scatters inelastically on the ion by way of the Coulomb interaction, and a secondary electron electron, q, is “knocked out” from an occupied atomic state, b. We will consider the case where both holes are in the outer-most valence subshell, $a = b = 5p^{-1}$. For knock-out to occur (and not just knock-up), the photon must have sufficient energy, $\Omega > |\epsilon_a| + |\epsilon_b|$, or more accurately, $\Omega > I_{\mathrm{DI}}$. This implies that the primary photoelectron will be in the continuum already before the KO takes place. Treating interactions occurring in the continuum requires special care concerning the boundary condition of the problem. Here, we have written explicitly the limit using $\varepsilon \to 0^+$, which enforces that the XUV field is zero at “minus infinity”, c.f. Ref. [23]. Consequently, the photoelectron will be of outgoing character (described by the coherent superposition over the p' states) before the “knock” occurs.

Evaluation of the limit in Eq. (31), leads to

$$\begin{aligned} M_{\mathrm{KO}} = \sum_{\lambda}^{|\ell_a \pm 1|} \Bigg\{ & \sum_{p'}^{\epsilon'_p<0} \frac{\langle qp|r_{12}^{-1}|bp'_\lambda\rangle\langle p'_\lambda|d_\Omega|a\rangle}{(a + \Omega - \epsilon'_{p,\lambda})} \\ & + \mathrm{p.v.} \int_0^\infty d\epsilon'_p \, \frac{\langle qp|r_{12}^{-1}|bp'_\lambda\rangle\langle p'_\lambda|d_\Omega|a\rangle}{(a + \Omega - \epsilon'_p)} \\ & - i\pi \, \langle qp|r_{12}^{-1}|bp^0_\lambda\rangle\langle p^0_\lambda|d_\Omega|a\rangle \Bigg\}, \end{aligned} \quad (32)$$

where the first line holds a summation over all intermediate bound excited states, p', λ with $\epsilon'_{p,\lambda} < 0$; the second line is a Cauchy principal value integral over all intermediate continuum states, p'_λ with $\epsilon'_p > 0$ but $\epsilon'_p \neq \epsilon_0$; and the third line is the “on-shell” contribution over the states $p^0_\lambda = p'_\lambda(\epsilon_0)$, where $\epsilon_0 = \epsilon_a + \Omega$. It is important to notice the imaginary number, i, on the resonant term, which signifies that the KO process carries a specific phase shift on its own. The summation on $\lambda = |\ell_a \pm 1|$ in Eq. (32) labels the angular momentum of the intermediate wave packet after the dipole transition from the initial state, a. The phase of the total KO process can then be written as the sum of the two final scattering phases and an intrinsic phase-shift due to the KO,

$$\arg M_{\mathrm{KO}} \sim \varphi_p(\epsilon_p) + \varphi_q(\epsilon_q) + \delta_{\mathrm{KO}}^{(a,b;p,q)}(\epsilon_p, \epsilon_q). \quad (33)$$

Explicitly, the phase of the KO process is determined by the ratio of the resonant above-threshold excitation and the sum of below-threshold excitation and non-resonant above-threshold excitation. In the limit of high energy, we expect the bound part to the small and the continuum contributions to be comparable, so that $\delta_{\mathrm{KO}} \to \pi/2$. The actual evaluation of the KO phase-shift is challenging, but we will provide an estimate in Sec. **??**.

4. Laser-assisted knock-out mechanism (LAKO)

We now turn to the laser-assisted KO diagrams, which we refer to as the LAKO processes, shown in Fig. 1 (f)–(h). First, we note that the probing of the primary electron, Fig. 1 (f) and (g), have different structure and can, therefore, not be joined as was done for the LASO process. For this reason, we have to consider all three LAKO diagrams separately as individual processes. In processes where the primary and secondary electrons are probed *after* KO, the lower parts of the diagrams are identical to the KO process, Fig. 1 (e).

Using energy conservation, Eq. (14), the matrix element for probing of the primary electron after IR, Fig. 1 (g), becomes

$$\begin{aligned} & M_{\mathrm{LAKO}}^{(p)}(\epsilon_p, \epsilon_q) = \quad (34) \\ & \lim_{\varepsilon_1,\varepsilon_2\to 0^+} \sum\!\!\!\!\!\!\!\int_{p',p''} \frac{\langle p|d_\omega|p''\rangle\langle qp''|r_{12}^{-1}|bp'\rangle\langle p'|d\Omega|a\rangle}{(\epsilon_a + \Omega - \epsilon'_p + i\varepsilon_1)(\epsilon_p \mp \omega - \epsilon''_p + i\varepsilon_2)}, \end{aligned}$$

where the first factor is indeed analogous to the KO process, Eq. (31), and the second factor describes absorption ($-\omega$) or emission ($+\omega$) of an IR photon toward the final state, p, with energy ϵ_p. Both interactions occur in the continuum and their evaluation requires setting the boundary condition of the interaction with the fields, $\Omega + i\varepsilon_1$ and $\mp\omega + i\varepsilon_2$ where $\varepsilon_1, \varepsilon_2 \to 0^+$, respectively. The first limit, ε_1, then gives a superposition similar to that in Eq. (32), but where the primary electron after KO is a superposition over all p'' states. This superposition is then treated using the second limit, ε_2, which enforces that the primary electron should be outgoing with an energy one IR photon away from the final state, $\epsilon''_p = \epsilon_p \mp \omega$. The details of this second step are identical to that of the “cc” transition in SPI and, therefore, leads to a cc phase-shift, c.f. Ref. [13]. The phase of the LAKO process for the primary electron contains

$$\begin{aligned} \arg M_{\mathrm{LAKO}}^{(p)} \sim\ & \delta_{\mathrm{KO}}^{(a,b;p,q)}(\epsilon_p \mp \omega, \epsilon_q) \\ & + \varphi_p(\epsilon_p \mp \omega) + \phi_{\mathrm{cc}}(\epsilon_p; \pm\omega) + \varphi_q(\epsilon_q), \end{aligned} \quad (35)$$

where both the KO phase-shift and the scattering phase of the primary electron are evaluated at one IR photon from the final state, while the secondary electron is evaluated at the final energy [quantum numbers correspond to Fig. 1 (e)].

Similarly, the denominator for probing of the secondary electron, Fig. 1 (h), is

$$\begin{aligned} & M_{\mathrm{LAKO}}^{(q)}(\epsilon_p, \epsilon_q) = \quad (36) \\ & \lim_{\varepsilon_1,\varepsilon_2\to 0^+} \sum\!\!\!\!\!\!\!\int_{p',q'} \frac{\langle q|d_\omega|q'\rangle\langle q'p|r_{12}^{-1}|bp'\rangle\langle p'|d_\Omega|a\rangle}{(\epsilon_a + \Omega - \epsilon'_p + i\varepsilon_p)(\epsilon_q \mp \omega - \epsilon'_q + i\varepsilon_q)}, \end{aligned}$$

and the phase contains

$$\begin{aligned}\arg M^{(q)}_{\mathrm{LAKO}} \sim\ & \delta^{(a,b;p,q)}_{\mathrm{KO}}(\epsilon_p,\epsilon_q\mp\omega)\\ &+\varphi_p(\epsilon_p)+\varphi_q(\epsilon_q\mp\omega)+\phi_{\mathrm{cc}}(\epsilon_q;\pm\omega),\end{aligned} \tag{37}$$

where, instead, the intermediate secondary electron is one photon away from its final energy.

The phase of LAKO process, including only probing after KO, takes an analogous form as for the case of the total LASO, Eq. (28), due to the different IR interaction strength with the two electrons. Following the same line of reasoning, the delay from the LAKO process (with IR after KO) becomes

$$\begin{aligned}\tau^{(\mathrm{after})}_{\mathrm{LAKO}} =& \frac{\Phi^{(\mathrm{emi})}_{\mathrm{LAKO}}-\Phi^{(\mathrm{abs})}_{\mathrm{LAKO}}}{2\omega}\\ =& \tfrac{1}{2\omega}\big\{\big[\delta^{(a,b;p,q)}_{\mathrm{KO}}(\epsilon_p+\omega,\epsilon_q)-\delta^{(a,b;p,q)}_{\mathrm{KO}}(\epsilon_p-\omega,\epsilon_q)\\ &+\delta^{(a,b;p,q)}_{\mathrm{KO}}(\epsilon_p,\epsilon_q+\omega)-\delta^{(a,b;p,q)}_{\mathrm{KO}}(\epsilon_p,\epsilon_q-\omega)\\ &+\varphi_p(\epsilon_p+\omega)-\varphi_p(\epsilon_p-\omega)\\ &+\varphi_q(\epsilon_q+\omega)-\varphi_q(\epsilon_q-\omega)\\ &+\phi_{\mathrm{cc}}(\epsilon_p;-\omega)-\phi_{\mathrm{cc}}(\epsilon_p;\omega)\\ &+\phi_{\mathrm{cc}}(\epsilon_q;-\omega)-\phi_{\mathrm{cc}}(\epsilon_q;\omega)\big]\times\tfrac{1}{2}\\ &+\delta\Phi^{\mathrm{LAKO}}_{\mathrm{weight}}(-\omega)-\delta\Phi^{\mathrm{LAKO}}_{\mathrm{weight}}(\omega)\big\},\end{aligned} \tag{38}$$

where we may identify a two-electron average of the KO delay, Wigner delay and cc delay plus a weighting correction,

$$\begin{aligned}\tau_{\mathrm{LAKO}} \approx\ & \tfrac{1}{2}[\tau^{(p)}_{\mathrm{W}}+\tau^{(q)}_{\mathrm{W}}+\tau^{(p)}_{\mathrm{KO}}+\tau^{(q)}_{\mathrm{KO}}\\ &+\tau^{(p)}_{\mathrm{cc}}+\tau^{(q)}_{\mathrm{cc}}]+\delta\tau^{\mathrm{LAKO}}_{\mathrm{weight}}.\end{aligned} \tag{39}$$

Our analysis for the lowest-order LAKO process is consistent with our heuristic approach, Eq. (12), as our results includes the average of the individual Wigner delays for the two electrons, $\frac{1}{2}(\tau^{(p)}_{\mathrm{W}}+\tau^{(q)}_{\mathrm{W}})$ and also the first correlation-induced delays due to the interaction of two active electrons, $\frac{1}{2}(\tau^{(p)}_{\mathrm{KO}}+\tau^{(q)}_{\mathrm{KO}})$. Already the lowest-order LAKO process is affected by correlation-induced phases and it requires a theory beyond static scattering phases. Similar to LASO, the LAKO process also introduces a cc delay that is similar to that of SPI and it shifts the delay smoothly depending on the relative interaction strength of the electron with the IR field.

The diagram in Fig. 1 (f) requires special attention. On the one hand, it interacts more strongly with the IR field due to the high momentum of the primary electron before the energy sharing of the KO applies, see Eq.(26), which would imply that it is an important effect. On the other hand, the absorption of an IR photon also changes the angular momentum of the primary electron, $\ell_{p''}=\ell_{p'}\pm1$, where dominant process is to increase the angular momentum to a $f-$wave. Thus, the primary electron is "pushed" away from the core ($5p$) and the corresponding overlap will slightly be smaller. The interesting aspect of probing before KO, is that it gives rise to a RABITT signal that corresponds to the SPI process,

$$\tau^{(\mathrm{before})}_{\mathrm{LAKO}}=\tau^{(\mathrm{SPI})}_{\mathrm{W}}+\tau^{(\mathrm{SPI})}_{\mathrm{cc}}. \tag{40}$$

One can see this by identifying that the second singularity occurs at the same energy for both absorption and emission arms of the RABITT process. This implies that any phase-shift brought by the KO process will cancel and the only remaining delay will be that of the SPI, i.e. before KO occurs. In this way, the SPI process will contaminate the LAKO process making it difficult to extract meaningful information about the DPI process.

In angle-integrated experimental measurements, not all degrees of freedom are observed and it is necessary to sum incoherently the probabilities for all angular paths. In addition, the processes where the secondary electron is more energetic than the primary, $\epsilon_q>\epsilon_p$, may prove important in the vicinity of equal energy sharing.

B. Correlation correction

1. *Shake-off mechanism*

The correlation correction term in Eqs. (11) and (12) is specific to the DPI mechanism. First, we estimate this term for the SO mechanism. We expand the SO diagram Fig. 1(a) beyond the lowest order of the perturbation theory over the inter-electron interaction [19]. This expansion includes the virtual Auger decay of the hole state c into two other holes a',b' and an electron q'. This dressing of the hole state is shown symbolically in Fig. 2(a) where we introduce an interacting (dressed) hole C shown by a double line. The corresponding non-interacting (bare) hole state c is displayed with a thin solid line. As is illustrated in Fig. 2(b), the dressed hole state includes an infinite summation of the diagonal self-energy diagrams Σ_c, shown in Fig. 2(c). In principle, this summation should also include non-diagonal self-energy $\Sigma_{c\neq c'}$. But these terms can be ignored for widely separated atomic shells, typical for noble gas atoms. In the diagonal approximation, the infinite summation of the diagrams of Fig. 2b can be performed by a geometric series and it leads to the following modification of Eq. (17):

$$\begin{aligned}M^{(a,b;p,q)}_{\mathrm{SO}}(\epsilon_p,\epsilon_q)\ =&\ \frac{\langle p|d_\Omega|c\rangle\langle c,q|r^{-1}_{12}|a,b\rangle}{(E-\epsilon_c-i\varepsilon)}\\ &\times\left(1-\frac{\Sigma_c(E)}{E-\epsilon_c-i\varepsilon}\right)^{-1}.\end{aligned} \tag{41}$$

Here $E=\epsilon_p-\Omega$ is the dressed hole energy which may differ from the bare hole energy ϵ_c. The diagonal self-energy

$$\Sigma_c(E)=\sum_{a'b'}\sum\!\!\!\!\!\!\!\int_{q'}\frac{\left|\langle c,q'|r^{-1}_{12}|a',b'\rangle\right|^2}{E-\epsilon_c-i\varepsilon}\ , \tag{42}$$

describes modification of the hole state, c, due to correlation. This modification includes a shift of the ionization potential relative to the bare hole energy ϵ_c as well as appearance of the discrete satellite lines and a continuous band in the spectrum of the singly charged ion states [19]. Each discrete line corresponds to a separate term in the sum $\sum_{a'b',q'}$ and the continuous band is due to the integral $\int_{q'}$. It is this continuous band in the singly charged ion spectrum that represents the doubly ionized states with the two holes a',b' and the two electrons p,q'. The imaginary infinitesimal in the denominator gives the

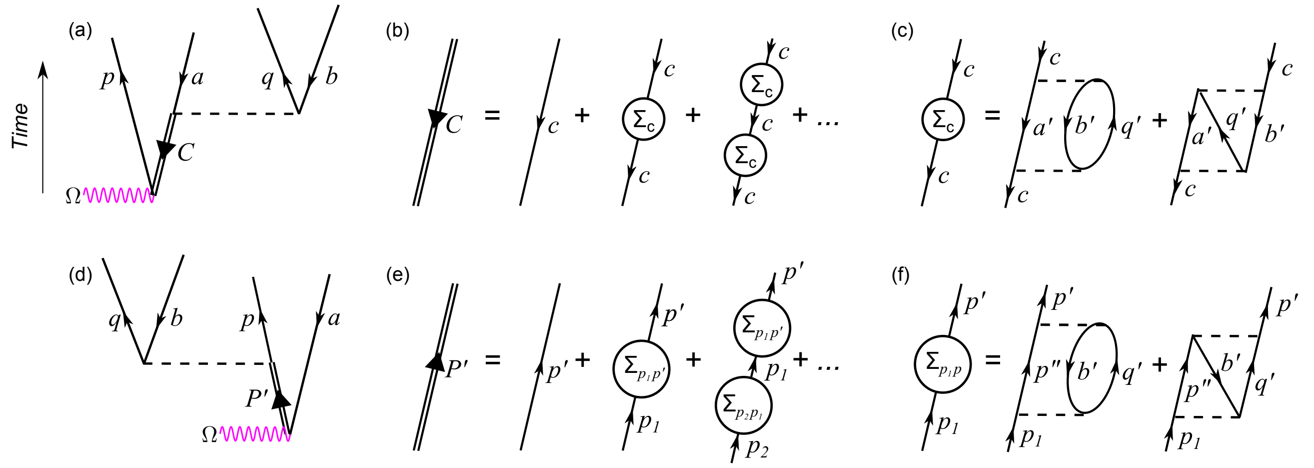

FIG. 2: Top row: Perturbation series of diagrams for the shake-off (SO) process (a); the correlated hole state (b); the diagonal hole self-energy (c); Bottom row: Perturbation series of diagrams for the knock-out (KO) process (d); the correlated electron state (e); the diagonal electron self-energy (f).

formal rule of bypassing the pole when Eq. (41) is evaluated at the energy E sufficient for the real Auger decay. This decay leads to the set of states ab, q identical to the final states of the shake-off diagram shown in Fig. 2a.

The imaginary part of the extra factor in the second line of Eq. (41), associated with the real Auger decay and the SO process, gives rise to an additional correlation correction of the phase of the DPI amplitude:

$$\begin{aligned}\delta_{\rm SO}^{(a,b;p,q)}(\epsilon_p,\epsilon_q) &= \arctan\frac{{\rm Im}\Sigma_c(E)}{{\rm Re}[E-\epsilon_c-\Sigma_c(E)]}\\ &\approx \arctan\frac{{\rm Im}\Sigma_c(E)}{E-\epsilon_c} \qquad (43)\end{aligned}$$

The approximate equality in the second line of Eq. (43) is satisfied under the condition that $|E-\epsilon_c| \gg |\Sigma_c(E)|$. This condition defines the part of the doubly ionized continuum that is far from the single ionization transition in which $E=\epsilon_c$. In other terms, it is the condition of the strongly forbidden Auger decay of the bare hole state c. This condition is satisfied in the case of $5s$ hole of Xe as is seen from Table I.

The DPI cross-section, corresponding to the SO process of Fig. 2a, differential with respect to the energy of the primary photoelectron p, is given by the following expression [19]:

$$\frac{d\sigma_c^{2+}}{dE_p} = \sigma_c^+\ \frac{1}{\pi}\frac{{\rm Im}\Sigma_c(E)}{|E-\epsilon_c-\Sigma_c(E)|^2} \approx \sigma_c^+\ \frac{1}{\pi}\frac{{\rm Im}\Sigma_c(E)}{|E-\epsilon_c|^2}\ . \qquad (44)$$

Here σ_p^+ is the single photoionization cross-section of the primary photoelectron. By solving this equation relative to ${\rm Im}\Sigma_c$, we can express the additional phase of the DPI amplitude due to the final state correlation in the following form:

$$\delta_{\rm SO}^{(a,b;p,q)}(\epsilon_p,\epsilon_q) = \arctan\frac{\pi}{\sigma_c^+}\frac{d\sigma_c^{2+}}{dE_p}|E-\epsilon_c|\ . \qquad (45)$$

We note that this phase correction can be expressed from the experimentally known cross-sections σ_p^+ and $d\sigma_c^{2+}/dE_p$.

Usually, the DPI channel is weak and the shake-off phase correction is small. In this case we can equate the arctangent function with its argument $\arctan(x) \simeq x$ when taking its derivative and simply write the corresponding time delay as

$$\tau_w^{ee-SO} = \frac{d\delta^{(\rm ee-SO)}(\epsilon_p,\epsilon_q)}{dE_p} \simeq \frac{\pi}{\sigma_c^+}\frac{d\sigma_c^{2+}}{dE_p} \qquad (46)$$

Here we only keep the energy derivative of the linear factor $E-\epsilon_c = E_p-\Omega-\epsilon_c$ and neglect all other derivatives.

Expansion of the KO diagram Fig. 1(e) beyond the lowest order perturbation theory is visualized in Fig. 2(d)-(f). This expansion includes a virtual knock-out process in which the primary photoelectron p' scatters inelastically into the state p" and creates an electron-hole pair b', q'. The dressed primary electron state is displayed by a double line in Fig. 2(d) and represents an infinite sum of the self-energy terms shown symbolically in Fig. 2(e). The photoelectron self-energy is exhibited in Fig. 2(f). Nonetheless, by restricting to the diagonal terms, we include important energy corrections to the dressed propagation of the photoelectron and provide a first estimate of the correlation-induced phase in the KO process. Summation of the infinite diagonal sequence of the diagrams in Fig. 2(e) leads to the following modification of Eq. (31)

$$M_{\rm KO}^{(a,b;p,q)}(\epsilon_p,\epsilon_q) = \sum\!\!\!\!\!\!\int_{p'} \frac{\langle q,p|r_{12}^{-1}|b,p'\rangle\langle p'|d_\Omega|a\rangle}{E-\epsilon'_p+i\varepsilon}\times \qquad (47)$$

$$\left[1+\sum\!\!\!\!\!\!\int_{p_1}\frac{\Sigma_{p_1p'}(E)}{E-\epsilon_{p_1}+i\varepsilon}+\sum\!\!\!\!\!\!\int_{p_1p_2}\frac{\Sigma_{p_2p_1}(E)}{E-\epsilon_{p_2}+i\varepsilon}\frac{\Sigma_{p_1p'}(E)}{E-\epsilon_{p_1}+i\varepsilon}+\ldots\right]$$

where $E=\epsilon_a+\Omega$ and the photoelectron self-energy is given by the following expression:

$$\Sigma_{pp'}(E) = \sum_{b'}\sum\!\!\!\!\!\!\int_{p''}\sum\!\!\!\!\!\!\int_{q'}\frac{\langle q,p''|r_{12}^{-1}|b,p\rangle\langle q,p''|r_{12}^{-1}|b,p'\rangle}{E-\epsilon_{p''}-\epsilon_{q'}+\epsilon_{b'}+i\varepsilon}\ . \qquad (48)$$

The integral terms in the second line of Eq. (47) can be written as

$$\sum\!\!\!\!\!\!\int_{p_1} \frac{\Sigma_{p_1 p'}(E)}{E-\epsilon_{p_1}+i\varepsilon} = \underbrace{\text{p.v.}\sum\!\!\!\!\!\!\int_{p_1} \frac{\Sigma_{p_1 p'}(E)}{E-\epsilon_{p_1}}}_{\text{Off}-\text{diagonal}} - \underbrace{i\pi\Sigma_{p'p'}(\epsilon_{p'})}_{\text{Diagonal}} \ .$$

We make the so-called pole approximation and neglect the principal value integral in the above expression. This leaves us with the sequence of diagonal self-energy terms $\Sigma_{p'p'} \equiv \Sigma_{p'}$ that can be summed by way of the geometrical progression:

$$1 - i\pi\Sigma_{p'}(\epsilon_{p'}) + [-i\pi\Sigma_{p'}(\epsilon_{p'})]^2 + \ldots = [1 + i\pi\Sigma_{p'}(\epsilon_{p'})]^{-1}$$

and then neglected the off-shell terms. Finally, we make the similar pole approximation to the KO diagram of Fig. 2(d) and retain the primary photoelectron with the on-shell energy $\epsilon_{p'_0} = \epsilon_p + \epsilon_q - \epsilon_b$. Then the expression for the correlation-induced phase of the KO amplitude becomes

$$\delta_{\text{KO}}^{(a,b;p,q)}(\epsilon_p, \epsilon_q) = \arctan \frac{-\pi \text{Re}\Sigma_{p'_0}(\epsilon_{p'_0})}{1 - \pi \text{Im}\Sigma_{p'_0}(\epsilon_{p'_0})} \qquad (49)$$

We note that if we neglect $\text{Im}\Sigma$ in the denominator, we arrive to the expression that gives correlation correction to the primary photoelectron scattering phase [20].

2. *Influence of the probe field*

Discussion about about probe field. Linear.

IV. TIME DELAY IN DPI OF XENON

Let us consider the kinematics corresponding to plots of Fig. 5 by Månsson et al. [17]. They used the photon energy $\omega = 40.1$ eV. At this photon energy, most of the shake-off intensity comes from the primary photoionization of the Xe $5s$ shell [21, 22]

In the case of the ^3P_q doubly charged ion, this corresponds to the total energy of the photoelectron pair of 7 eV and the fixed energy slow electron takes 2 eV. So the fast photoelectron takes 5 eV. With the HF energy $E_{5s} = 25.7$ eV, this makes $\epsilon = 35.1$ eV and $\varepsilon - E_i \simeq 10$ eV. Let us assume that the whole continuous part of the satellite spectrum takes about 10% of the main line and this spectrum is spread over the 1 Ry = 0.5 au energy band. With these estimates, $\tau_{SO} \simeq 0.2\pi$ au = 15 as. A more accurate estimate of the SO term can be done by using the experimental cross-sections for single and double photoionization.

The full time-delay in DPI under the SO model is therefore

$$\tau = \frac{1}{2}\frac{\partial}{\partial\epsilon_p}\eta_{5s\to Ep}(\epsilon_p) + \frac{1}{2}\frac{\partial}{\partial\epsilon_q}\eta_{5p\to Ed}(\epsilon_q) + \tau_{SO} \qquad (50)$$

The time delay due to the phase factors of individual photoelectrons can be estimated using the data by Kheifets [18]:

$$\frac{\partial}{\partial\epsilon_p}\eta_{5s\to Ep}\Big|_{\epsilon_p = 5\text{ eV}} = 220 \text{ as} \quad , \quad \frac{\partial}{\partial\epsilon_q}\eta_{5p\to Ed}\Big|_{\epsilon_q = 2\text{ eV}} = 550 \text{ as}$$

Hence,

$$\tau = \frac{1}{2}\frac{\partial}{\partial\epsilon_p}\eta_{5s\to Ep}(\epsilon_p) + \frac{1}{2}\frac{\partial}{\partial\epsilon_q}\eta_{5p\to Ed}(\epsilon_q) + \tau_{SO} = 110 + 275 + 15 =$$

These are numerical values for photoelectron scattering on Xe$^+$ $5p^5$ in d-partial wave. We see that phase corrections are not different from corresponding self-energy values when multiplied by $-\pi$. When the phase derivative plot is converted to the time delay it rarely exceeds 10as.

The time delay due to the phase factors of individual photoelectrons can be estimated using the data by Kheifets [18]:

$$\frac{\partial}{\partial\epsilon_p}\eta_{4d\to Ef}\Big|_{\epsilon_p = 5\text{ eV}} = 190 \text{ as} \quad , \quad \frac{\partial}{\partial\epsilon_q}\eta_{5p\to Ed}\Big|_{\epsilon_q = 2\text{ eV}} = 550 \text{ as}$$

It is more prudent to use $\eta_{5p\to Ef}$ phase but I only have the HF value for this phase that returns 203 as time delay.

V. CONCLUSION

Acknowledgments

---

[1] J. S. Briggs and V. Schmidt, *Differential cross sections for photo-double-ionization of the helium atom*, J. Phys. B **33**(1), R1 (2000).

[2] L. Avaldi and A. Huetz, *Photodouble ionization and the dynamics of electron pairs in the continuum*, J. Phys. B **38**(9), S861 (2005).

[3] J. H. McGuire, *Electron Correlation Dynamics in Atomic Collisions*, Cambridge Monographs on Atomic, Molecular and Chemical Physics (Cambridge University Press, Cambridge, 1997).

[4] T. Schneider, P. L. Chocian, and J.-M. Rost, *Separation and identification of dominant mechanisms in double photoionization*, Phys. Rev. Lett. **89**, 073002 (2002).

[5] A. Knapp, A. Kheifets, I. Bray, T. Weber, A. L. Landers, S. Schössler, T. Jahnke, J. Nickles, S. Kammer, O. Jagutzki, et al., *Mechanisms of photo double ionization of helium by 530 ev photons*, Phys. Rev. Lett. **89**, 033004 (2002).

[6] M. Schultze *et al*, *Delay in Photoemission*, Science **328**(5986), 1658 (2010).

[7] K. Klünder *et al*, *Probing single-photon ionization on the attosecond time scale*, Phys. Rev. Lett. **106**(14), 143002 (2011).

[8] D. Guénot, K. Klünder, C. L. Arnold, D. Kroon, J. M. Dahlström, M. Miranda, T. Fordell, M. Gisselbrecht, P. Johnsson, J. Mauritsson, et al., *Photoemission-time-delay measurements and calculations close to the 3s-ionization-cross-section minimum in ar*, Phys. Rev. A **85**, 053424 (2012).

[9] P. M. Paul, E. S. Toma, P. Breger, G. Mullot, F. Augé, P. Balcou, H. G. Muller, and P. Agostini, *Observation of a train of attosecond pulses from high harmonic generation*, Science **292**(5522), 1689 (2001).

[10] S. Nagele, R. Pazourek, J. Feist, K. Doblhoff-Dier, C. Lemell, K. Tökési, and J. Burgdörfer, *Time-resolved photoemission by attosecond streaking: extraction of time information*, J. Phys. B **44**(8), 081001 (2011).

[11] S. Nagele, R. Pazourek, J. Feist, and J. Burgdörfer, *Time shifts in photoemission from a fully correlated two-electron model system*, Phys. Rev. A **85**, 033401 (2012).

[12] A. S. Kheifets and I. A. Ivanov, *Delay in atomic photoionization*, Phys. Rev. Lett. **105**(23), 233002 (2010).

[13] J. Dahlström, D. Guénot, K. Klünder, M. Gisselbrecht, J. Mauritsson, A. L. Huillier, A. Maquet, and R. Taïeb, *Theory of attosecond delays in laser-assisted photoionization*, Chem. Phys. **414**, 53 (2012).

[14] J. M. Dahlstr.m, A. L.Huillier, and A. Maquet, *Introduction to attosecond delays in photoionization*, Journal of Physics B: Atomic, Molecular and Optical Physics **45**(18), 183001 (2012).

[15] A. S. Kheifets, I. A. Ivanov, and I. Bray, *Timing analysis of two-electron photoemission*, J. Phys. B **44**(10), 101003

[16] R. Pazourek, J. Feist, S. Nagele, and J. Burgdörfer, *Attosecond streaking of correlated two-electron transitions in helium*, Phys. Rev. Lett. **108**, 163001 (2012).

[17] E. P. Månsson, D. Guénot, C. L. Arnold, D. Kroon, S. Kasper, J. M. Dahlström, L. E., A. S. Kheifets, A. L'Huillier, S. L. Sorensen, et al., *Double ionization of xenon probed on the attosecond time scale*, Nature p. submitted (2013).

[18] A. S. Kheifets, *Time delay in valence shell photoionization of noble gas atoms*, ArXiv e-prints p. 1302.4495 (2013).

[19] M. Y. Amusia and A. S. Kheifets, *Effect of correlations on the photoelectron spectrum of atom*, Sov. Phys. -JETP **59**, 710 (1984).

[20] M. Y. Amusia, N. A. Cherepkov, L. V. Chernysheva, D. M. Davidovi'c, and V. Radojevi¸ *Slow-electron elastic scattering on argon*, Phys. Rev. A **25**(1), 219 (1982).

[21] J. E. Hansen and W. Persson, *Revised analysis of singly ionized xenon, Xe II*, Physica Scripta **36**(4), 602 (1987).

[22] A. S. Kheifets and M. Y. Amusia, *Relativistic ab initio calculation of the xenon* $5s$ *ionization spectra for the* (γ,e) *and (e,2e) reactions*, Phys. Rev. A **46**, 1261 (1992).

[23] J. M. Dahlström, A. L. Huillier, and A. Maquet *Introduction to attosecond delays in photoionization*, J. Phys. B **45**, 183001 (2012).

[24] C. Pan, and H. P. Kelly, *Photoionization cross sections of the Ar atom for production of singly and doubly charged ions near the 2p threshold*, Phys. Rev. A **39**, 6232 (1989).

[25] Y. Ralchenko, A. E. Kramida, J. Reader, and NIST ASD Team, *NIST Atomic Spectra Database (version 3.1.5)*, Tech. Rep., National Institute of Standards and Technology, Gaithersburg, MD. (2011), URL `http://physics.nist.gov/asd`.